TOPICAL REVIEW — Fundamental physics research in lithium batteries

Understanding oxygen reactions in aprotic Li-O_2 batteries*

Shunchao Ma(马顺超)[1,2,†], Yelong Zhang(张业龙)[1,2,†], Qinghua Cui(崔清华)[1,2], Jing Zhao(赵婧)[1,2], and Zhangquan Peng(彭章泉)[1,‡]

[1] State Key Laboratory of Electroanalytical Chemistry, and Institute of Applied Chemistry, Chinese Academy of Sciences, Changchun 130022, China
[2] University of Chinese Academy of Sciences, Beijing 100039, China

(Received 2 June 2015; revised manuscript received 16 July 2015; published online 30 November 2015)

Although significant progress has been made in many aspects of the emerging aprotic Li-O_2 battery system, an in-depth understanding of the oxygen reactions is still underway. The oxygen reactions occurring in the positive electrode distinguish Li-O_2 batteries from the conventional Li-ion cells and play a crucial role in the Li-O_2 cell's performance (capacity, rate capability, and cycle life). Recent advances in fundamental studies of oxygen reactions in aprotic Li-O_2 batteries are reviewed, including the reaction route, kinetics, morphological evolution of Li_2O_2, and charge transport within Li_2O_2. Prospects are also provided for future fundamental investigations of Li-O_2 chemistry.

Keywords: Li-O_2 batteries, oxygen reduction reactions, oxygen evolution reactions, kinetics

PACS: 82.47.Aa, 71.38.Ht, 82.45.Jn **DOI:** 10.1088/1674-1056/25/1/018204

1. Introduction

Aprotic Li-O_2 batteries have much greater gravimetric energy density than the traditional Li-ion technologies, making them promising candidates for future energy storage systems.[1–9] The aprotic Li-O_2 battery, initially introduced by Abraham *et al.*,[10] is typically composed of a Li metal anode, an aprotic Li^+ electrolyte, and an air cathode, in which the active material (O_2) of the cathode is drawn from the atmosphere. Currently, the aprotic Li-O_2 battery development encounters substantial scientific and technological challenges that impede its practical applications including high charging over-potential (which limits round-trip efficiency),[11,12] poor stability of cathodes and electrolytes (which decreases cycle life),[13–15] deposition of insulating Li_2O_2 product (which degrades the cell's capacity),[16,17] and safety issues associated with Li metal anodes.[18,19] Most of these challenges are related to the oxygen reactions occurring in the positive electrodes of the aprotic Li-O_2 cells. Therefore, to tackle these issues effectively, an in-depth understanding of the oxygen reaction mechanisms is crucial. In this review, we summarize a few fundamental aspects of the oxygen electrode reactions in aprotic Li-O_2 batteries, including the reaction route, kinetics, morphological evolution of Li_2O_2 and charge transport within Li_2O_2.

2. Oxygen reduction reactions (ORRs) in aprotic Li-O_2 batteries

2.1. ORR mechanisms

Without considering any of the possible parasitic side reactions, the fundamental chemistry of an aprotic Li-O_2 battery during discharge undergoes these possible elementary reactions:[20–24]

$$e^- + O_2 \rightarrow O_2^-, \quad (1)$$

$$Li^+ + O_2^- \rightarrow LiO_2, \quad (2)$$

$$Li^+ + e^- + LiO_2 \rightarrow Li_2O_2, \quad (3)$$

$$LiO_2 + LiO_2 \rightarrow Li_2O_2 + O_2. \quad (4)$$

To identify the ORR mechanisms in aprotic Li-O_2 cells, several research groups investigated the ORRs with multiple techniques including voltammetry,[20–23] electrochemical surface-enhanced Raman spectroscopy (EC-SERS),[24–26] differential electrochemical mass spectrometry (DEMS),[27] etc. For instance, Laoire *et al.* studied ORRs in various organic solvents (such as acetonitrile [ACN] and dimethylsulfoxide [DMSO]) containing various cations (such as tetrabutylammonium [TBA^+] and alkali metal ions of Li^+, Na^+, and K^+) using cyclic voltammetry.[20,21] Meanwhile, the reaction between O_2^- and Li^+ was also investigated by Peng *et al.* (Fig. 1). With the addition of Li^+, the reduction peak appears at higher potentials, and with increasing Li^+ concentration, the magnitude of the new peak increases at the expense of the area un-

*Project supported by the Recruitment Program of Global Youth Experts of China, the Strategic Priority Research Program of the Chinese Academy of Sciences (Grant No. XDA09010401), the Science and Technology Development Program of Jilin Province, China (Grant No. 20150623002TC), and the Natural Science Foundation of Jiangsu Province, China (Grant No. BK20131139).

†These authors contributed equally.

‡Corresponding author. E-mail: zqpeng@ciac.ac.cn

© 2016 Chinese Physical Society and IOP Publishing Ltd

der the original O_2 reduction peak, meaning that electrochemical reduction is followed by a chemical step. This subsequent chemical reaction severely depletes the amount of O_2^-, leading to a shift of the potential toward higher voltages. These observations are consistent with the proposed ORR mechanisms illustrated by Eqs. (1)–(4), i.e., O_2 is first reduced to intermediate O_2^- via a one-electron process (Eq. (1)), the O_2^- binds with Li^+ ions forming LiO_2, an unstable intermediate (Eq. (2)). Then, LiO_2 further transforms to Li_2O_2 through either electrochemical reduction (Eq. (3)) or chemical disproportionation (Eq. (4)). Abraham *et al*. also used hard soft acid base (HSAB) theory to clarify this ORR process. According to the HSAB theory, alkali metal cations such as Li^+ ions, which represent hard acids, cannot efficiently stabilize O_2^-, a relatively soft base. Hence, the unstable intermediate LiO_2 is prone to disproportionation, forming Li_2O_2, because O_2^{2-} is a strong base.[20,21,28]

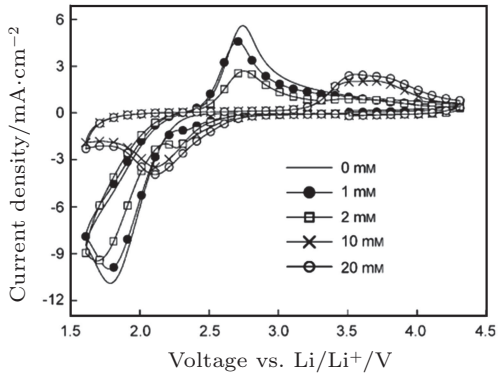


Fig. 1. Cyclic voltammetry at a roughened Au electrode in O_2 saturated 0.1 $MnBu_4NClO_4$ in CH_3CN containing various concentrations of $LiClO_4$ as indicated. The scan rate was 1 V·s^{-1}.[24]

The proposed ORR mechanisms (Eqs. (1)–(4)) were investigated by Peng *et al*. using EC-SERS.[24] With this spectroscopy-based technique, the reaction products and intermediates, which are crucial to the formulation of the ORR mechanisms in the aprotic Li^+ electrolyte, were identified directly. As shown in Fig. 2, at the initial stage of ORRs, two newly formed species, LiO_2 (peak 2) and Li_2O_2 (peak 3), can be identified; they are absent at open circuit potential, where no ORR takes place. Moreover, with the elapse of time, the signal associated with LiO_2 gradually decreases and vanishes, and only the signal of Li_2O_2 remains. These observations clearly demonstrate that the unstable LiO_2 can transform to Li_2O_2 via disproportionation, supporting the reaction mechanisms of either Eqs. (1), (2), and (4) or Eqs. (2) and (4).

In addition, McCloskey *et al*. employed cyclic voltammetry (CV) and differential electrochemical mass spectrometry (DEMS) to study the oxygen reactions in aprotic Li-O_2 cells with a lithium bis(trifluoromethanesulfonyl)imide(LiTFSI)-dimethoxyethane (DME) electrolyte.[27] Interestingly, only one peak for ORRs was observed (Fig. 3(a)). Their observations differ from many published results that demonstrated multiple peaks of ORRs in the cyclic voltammograms (CVs) and those peaks were attributed to one-electron processes.[20,21] McCloskey *et al*. argued that the extra reduction peaks in CVs are due to the presence of impurities, e.g., H_2O. Moreover, the $\sim 2e^-/O_2$ process forming Li_2O_2 has been confirmed by DEMS experiments, as exhibited in Fig. 3(b). This means that once the LiO_2 is formed, it quickly transforms to Li_2O_2 by reaction (Eq. (3)) or reaction (Eq. (4)), and it cannot be thermodynamically stable, contrary to the suggestions of others.[20,22–24]

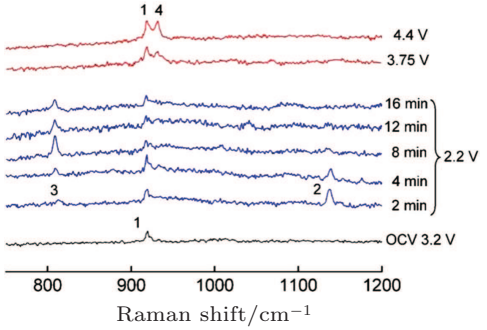


Fig. 2. *In situ* SERS during O_2 reduction and re-oxidation on Au in O_2-saturated 0.1 M $LiClO_4$–CH_3CN. Spectra collected at a series of times and at the reducing potential of 2.2 V versus Li/Li^+ followed by other spectra at the oxidation potentials shown. The peaks are assigned as follows: 1) C–C stretch of CH_3CN at 918 cm^{-1}, 2) O–O stretch of LiO_2 at 1137 cm^{-1}, 3) O–O stretch of Li_2O_2 at 808 cm^{-1}, and 4) Cl–O stretch of ClO_4^- at 931 cm^{-1}.[24]

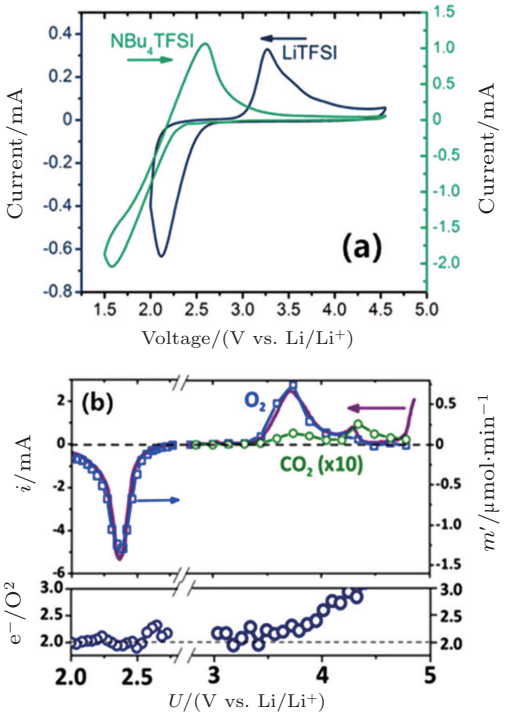


Fig. 3. (a) CVs showing O_2 reduction and re-oxidation in 0.5 M NBu_4TFSI (green, right ordinate) and 1 M LiTFSI (blue, left ordinate). (b) Linear sweep voltammetry at 0.5 mV/s using the DEMS cell (XC 72 carbon cathode, 1 M LiTFSI in DME). The solid line is the current, and the points are O_2 (and CO_2) measured by the DEMS. e^-/O_2 was determined by comparing the current to the moles of O_2 consumed or evolved.[27]

Early CV studies of ORRs in aprotic solvents reported by Laoire *et al*. are excellent, but the reaction products and intermediates cannot be identified with certainty by these conventional electrochemical methods;[28] therefore, the mechanisms that were proposed based on CV measurements are questionable. The extra peaks of ORRs in CVs may be due to the existence of H_2O in the electrolyte, as suggested by a recent work,[29] and the effects of residual H_2O (or any proton sources) need further clarification. By EC-SERS, the ORR intermediate LiO_2 has been detected directly, which is very beneficial for the formulation of the ORR mechanisms. Spectroscopy-based techniques will continue to play a key role in better understanding the ORRs in various aprotic Li-O_2 batteries that incorporate a broad range of aprotic electrolyte solvents. However, DEMS experiments demonstrate that an overall two-electron process is obtained within the time resolution (seconds) of this technique, which means that LiO_2 may not be a stable intermediate and could rapidly transform to Li_2O_2. This contradiction between the DEMS and SERS results needs further study. So far, there is no consensus on the path of LiO_2 transformation to Li_2O_2 under the conditions of Li-O_2 cell operation, i.e., whether it is dominated by electrochemical reduction or chemical disproportionation. Further investigations are urged, seeking a better understanding of ORRs in aprotic Li-O_2 batteries.

2.2. ORR kinetics

Understanding the intrinsic ORR kinetics and transport limitations associated with Li_2O_2 formation is crucial to the development of aprotic Li-O_2 batteries with the desired rate capabilities. To explore ORR kinetics, Gallant *et al*. investigated the ORR over-potentials on a carbon nanotube-based cathode by using galvanostatic and potentiostatic intermittent titration (PITT) techniques.[30] Under potentiostatic conditions, the average current increases in magnitude as the voltage is reduced from 2.76 V to 2.0 V (Fig. 4(a)). The acquired 2.76 V is the maximum potential at which nucleation of Li_2O_2 on CNTs occurs, corresponding to the PITT discharge at open circuit potential, as shown in Fig. 4(b). These results were further validated by a galvanostatic discharge test (Fig. 4(c)). Moreover, the discharge potential plateaus present a linear relationship with $\log i_{\text{galvano}}$, described in a Tafel curve (Fig. 4(d)), confirmed with a kinetically controlled ORR procedure. Notably, the measured Tafel slope differs from the reported results for other types of cathodes.[31] Although the physical origin of this difference is not understood, the different Tafel slopes observed on various carbon surfaces at low Li_2O_2 coverage may reflect different nucleation kinetics of Li_2O_2.

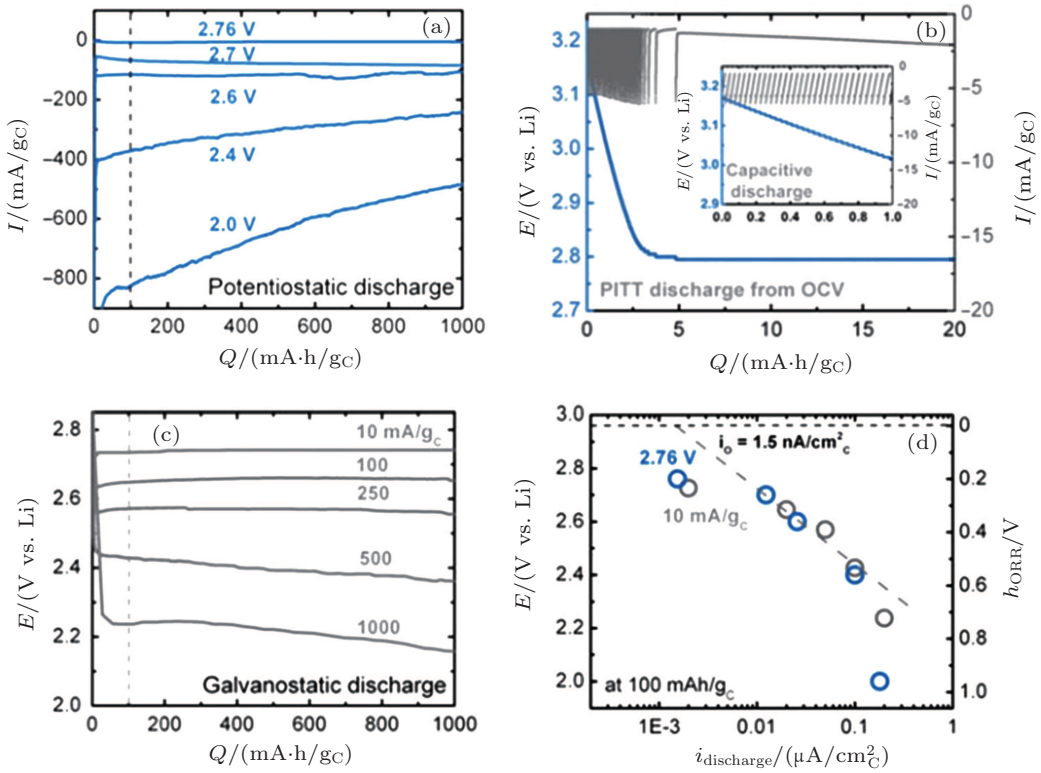


Fig. 4. (a) Current vs. capacity of CNT electrodes discharged potentiostatically over a range of potentials between 2.0 V and 2.76 V. (b) PITT discharge of CNT electrodes from an open circuit ($\sim$ 3.15 V) with a voltage step of 5 mV and a current cutoff per step of 1 mA/g_C. Inset: zoom-in of the PITT response in the capacity range below 1 mA·h/g_C, where the current corresponds to only capacitive discharge. (c) Voltage vs. capacity of CNT electrodes discharged galvanostatically between 10 mA/g_C and 1000 mA/g_C. (d) Tafel plot of voltage vs. carbon true surface area-normalized current for electrodes discharged potentiostatically (blue circles) from (a) and galvanostatically (gray circles) from (c).[30]

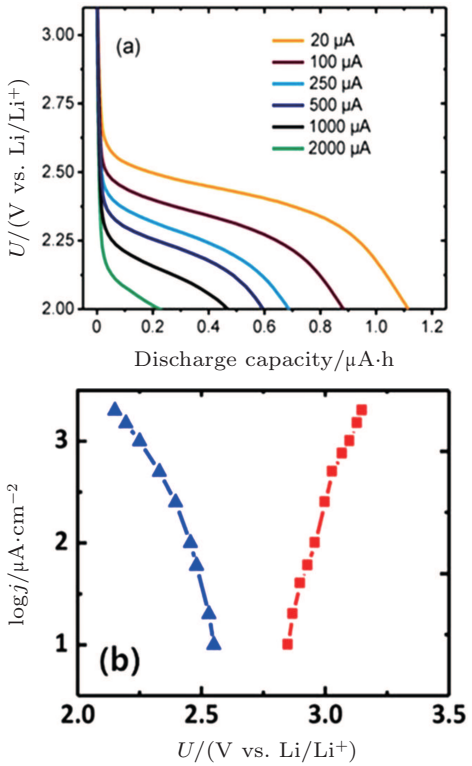


Fig. 5. (a) Output potential during Li-O_2 galvanostatic discharge in the bulk electrolysis cell at the current densities given in the legend. (b) Experimental Tafel plots for Li-O_2 discharge (ORR, blue triangles) and for charging following discharge (OER, red squares).[32]

Many studies of discharge behavior and kinetic process using typical Swagelok-type cells with carbon cathodes were reported in the literatures,[30,31] however, Viswanathan *et al.* argued that these results may fully mask the fundamental kinetic behavior due to the cell's intrinsic impedance. It is critical to eliminate the cell *iR* drop for measuring the fundamental kinetic over-potential. Therefore, Viswanathan and associates estimated the kinetic over-potentials by using a bulk electrolysis cell with a flat, polished, small-surface glassy carbon (GC) electrode.[32] Figure 5(a) shows galvanostatic discharge plots of Li-O_2 cell at various current densities i in the bulk electrolysis cell. The initial drop in potential is attributed to the kinetic over-potential, a linear decrease in potential with $Q_{\rm dis}$ is ascribed to an *iR* drop through the thickening Li_2O_2 film on the GC surface, and a "sudden death" is characterized by a rapid decrease in U. These authors discussed only the initial drop of potential U and its i dependence to probe the real kinetic behavior, because charge transport limitations for Li_2O_2 growth dominate the electrochemistry during the later discharge. Figure 5(b) is the Tafel plot for the cell's cycle, wherein it is plain to see that the kinetic over-potentials for discharge and recharge procedures are extremely small. These results imply that the electrical efficiency of a Li-O_2 battery is high in a discharge-recharge cycle if the battery is limited only by the kinetic over-potential.

2.3. Li_2O_2 morphology

The reported morphology of Li_2O_2 formed on a cathode is also controversial. Viswannathan *et al.* reported homogeneous films of Li_2O_2 deposited on a small-surface GC cathode

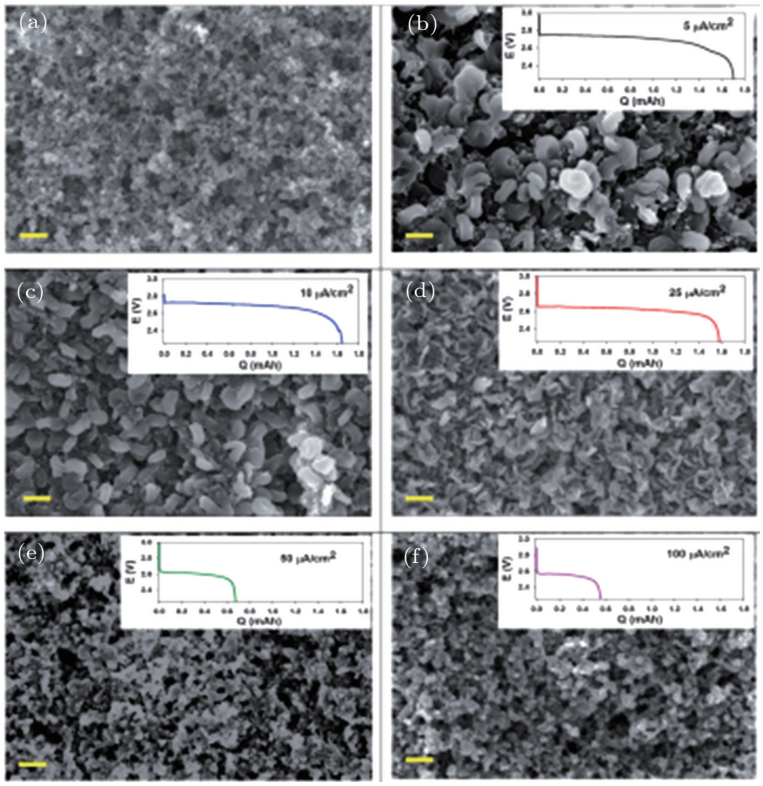


Fig. 6. FESEM images at a magnification of 20000 of (a) the pristine cathode and after full discharge at (b) 5 mA/cm^2, (c) 10 mA/cm^2, (d) 25 mA/cm^2, (e) 50 mA/cm^2, and (f) 100 mA/cm^2, with the corresponding discharge curves shown as insets. Scale bar = 400 nm.[16]

in an electrolysis cell, observed by atomic force microscopy (AFM).[33] Adams *et al*. also observed the formation of a quasi-amorphous peroxide film at high current rates, as shown in Figs. 6(e) and (f).[16] However, at low current rates, toroid-shaped Li_2O_2 products have been found (Figs. 6(b)–6(d)) on a pristine carbon cathode (Fig. 6(a)). Obtaining such small, poorly crystalline particles at high current density was ascribed to the direct second electro-reduction pathway (Eq. (3)) due to the stronger adsorption of LiO_2 onto the Li_2O_2 substrate at this high current rate.[16]

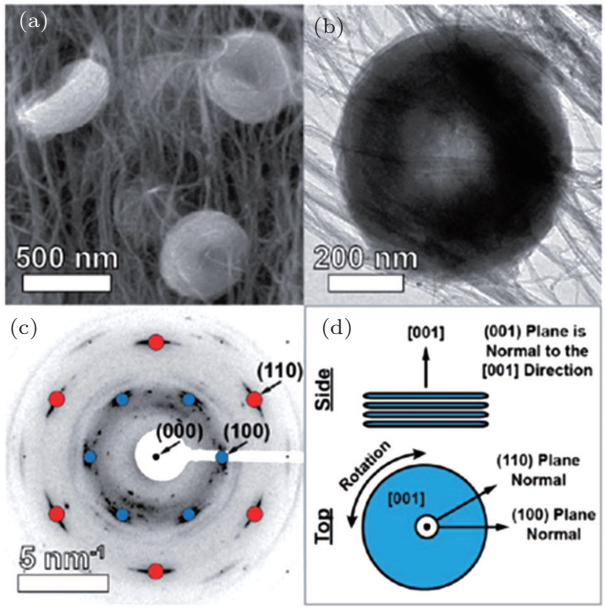


Fig. 7. Electron diffraction investigation of individual Li_2O_2 particles. (a) SEM and (b) bright-field TEM images of toroid particles. (c) Simulated Li_2O_2 [001] zone axis superimposed over an experimental diffraction pattern for the particle pictured in panel (b). (d) Side-view and top-view schematics of a stack of crystallite plates.[34]

Other researchers also reported that the toroid-like Li_2O_2 particles are formed on various types of carbon cathodes, especially at low discharge current density.[30,34,35] For instance, Shao-Horn and colleagues revealed the morphology evolution of these toroid-like products by using transmission electron microscopy (TEM), the formation originally began with the nucleation of small particles on the side wall of CNT and evolved upon continued discharge. The TEM investigation also showed that these toroids are highly crystalline with the Li_2O_2 (0001) facet normal to the axis of the toroid as shown in Fig. 7. It is worth noting that this observation of toroids has triggered much controversy about ORR mechanisms in aprotic Li-O_2 batteries, because the morphology is totally different from the films observed in an electrolysis cell, and the toroid-like Li_2O_2 particles with poor electrical conductivity and large size (several hundred nanometers) can be electrochemically oxidized. In a recent work, the formation of the Li_2O_2 toroids was ascribed to the existence of H_2O impurity,[29] i.e., H_2O induces some solubility of LiO_2 due to its high acceptor number, which helps validate the solution mechanism for Li_2O_2 formation proposed by others.[16]

3. Oxygen evolution reactions (OER) in aprotic Li-O_2 batteries

3.1. OER mechanisms

Understanding the Li_2O_2 oxidation reactions is also crucial to the development of Li-O_2 cells with high energy efficiency and long cycle life. However, the Li_2O_2 decomposition reactions at the cathode are complex and have not been fully understood so far. As for ORRs, the following mechanisms for Li_2O_2 oxidation reactions have been proposed:[24,30,31,36–38]

$$Li_2O_2 \rightarrow O_2 + 2e^- + 2Li^+, \quad (5)$$

$$Li_2O_2 \rightarrow LiO_2 + e^- + Li^+, \quad (6)$$

$$LiO_2 \rightarrow O_2 + e^- + Li^+, \quad (7)$$

$$2LiO_2 \rightarrow Li_2O_2 + O_2. \quad (8)$$

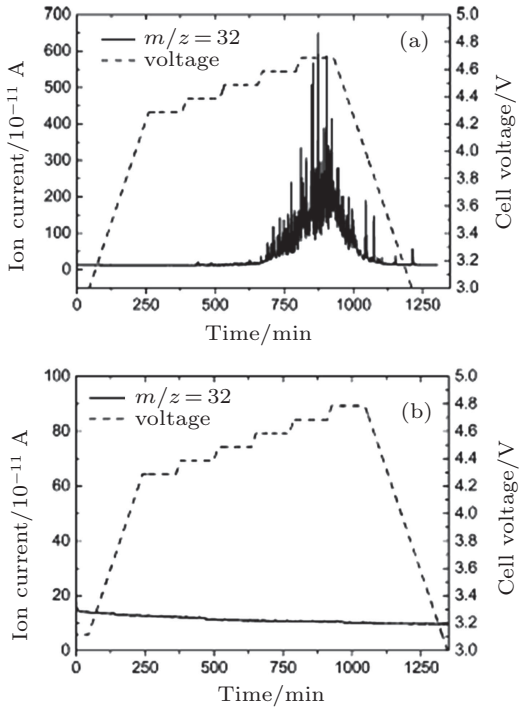


Fig. 8. Variation of ion current corresponding to O_2 evolution as a function of time. The voltage was increased by 100 mV every 120 min. (a) Electrode with Li_2O_2 and (b) electrode without Li_2O_2.[36]

The electrochemical decomposition of Li_2O_2 to Li^+ and O_2 (Eq. (5)) during charging has been qualitatively demonstrated by Ogasawara *et al*.[36] using *in situ* DEMS that showed the expected O_2 evolution. This work is the first piece of experimental evidence about the reversibility of the aprotic Li-O_2 cells, and it indicates the possibility of the successful operation of a rechargeable Li-O_2 battery (Fig. 8). To explore OER mechanisms directly, *in situ* SERS and DEMS studies were conducted by Peng *et al*.[24] Figure 2 shows the EC-SERS results of Li_2O_2 decomposition, in addition to its

formation. After applying a reducing potential of 2.2 V until only Li_2O_2 was presented, the potential was switched to 3.75 V then to 4.4 V to decompose Li_2O_2. The SERS spectra collected at these oxidation potentials showed no evidence of LiO_2, indicating that Li_2O_2 decomposed directly to O_2 and Li^+ without passing through LiO_2 as an intermediate. Quantitative DEMS study showed the results of a Li_2O_2 electrode charged with successive current steps (Fig. 9). As the current is increased, a concomitant increase occurs in both the cell potential and the $m/z = 32$ signal, due to the O_2 evolution on decomposing Li_2O_2 during charging. DEMS results revealed that Li_2O_2 decomposes directly in an one-step process to O_2, that is, through reaction (5), which is consistent with the SERS results.

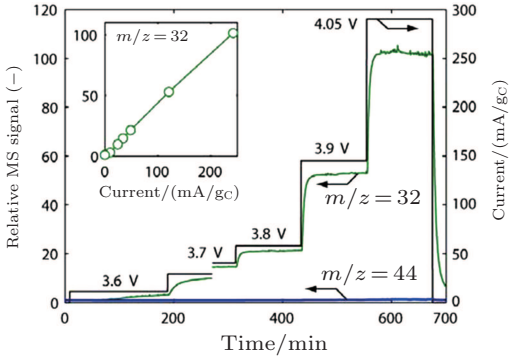


Fig. 9. Differential electrochemical mass spectrometry on oxidation of Li_2O_2, signal for $m/z = 32$ (O_2) and $m/z = 44$ (CO_2) in response to stepwise increase in oxidation current. Inset: $m/z = 32$ signal as a function of oxidation current, showing proportional relationship.[24]

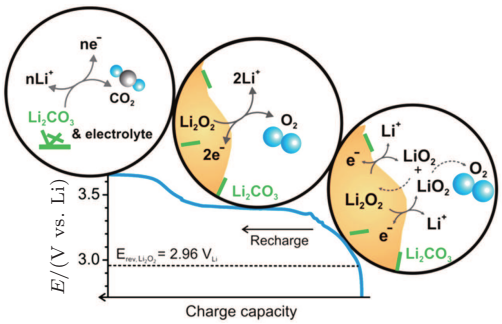


Fig. 10. Proposed reaction mechanism of Li-O_2 recharge. The OER process associated with stage I (sloping and catalyst-insensitive) is attributed to a de-intercalation process via a solid-solution route from the outer part of Li_2O_2 to form LiO_2-like species on the surface ($Li_2O_2 \rightarrow LiO_2 + Li^+ + e^-$), where LiO_2-like species disproportionate to evolve O_2 ($LiO_2 + LiO_2 \rightarrow Li_2O_2 + O_2$), yielding an overall $2e^-/O_2$ OER process ($Li_2O_2 \rightarrow 2Li^+ + O_2 + 2e^-$). The OER process at the flat potential plateau (stage II) is attributed to the oxidation of bulk Li_2O_2 particles to form Li^+ ions and O_2 ($Li_2O_2 \rightarrow 2Li^+ + 2e^- + O_2$) via a two-phase transition. Lastly, a rising charge plateau after stage II has been assigned to the decomposition of carbonate-type byproducts and electrolyte.[31]

However, Lu and Shao-Horn[31] speculated that the rising potential in the oxidation process is due to different mechanisms for OER (Fig. 10): a low over-potential process corresponds to Li de-intercalation at the surface (Eq. (6)) followed by chemical disproportionation (Eq. (8)), and a higher over-potential mechanism for an unspecified bulk oxidation process (Eq. (5)). Gallant *et al.*[30] also proposed an alternative route for the Li_2O_2 oxidation process, as shown in Fig. 11: the lower over-potential is simply attributed to the $1e^-$ de-lithiation process; and the subsequent higher potential plateau is attributed to the oxidation of bulk Li_2O_2. In recent studies, Yang *et al.*[37] observed the existence of LiO_2-like species in discharged products. These LiO_2-like species were ascribed to the superoxide-like oxygen rich surfaces of Li_2O_2 and/or small Li_2O_2 clusters, indicating a possible reaction (Eq. (7)). However, the decomposition path of Li_2O_2 through LiO_2 has not been clarified, and the most compelling argument against these mechanisms is simply that they cannot be shown to agree with DEMS results, which show an $e^-/O_2 \sim 2$ process (Eq. (5)) for charging. Thus, we still have the key puzzle regarding the true mechanisms of OER in aprotic Li-O_2 batteries.

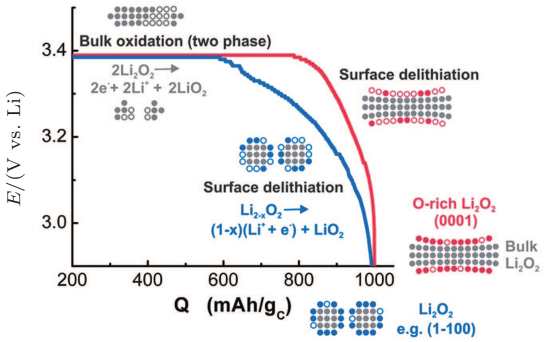


Fig. 11. Proposed charging processes for Li_2O_2, with disc (gray/red, typical dimensions $\sim$ 50 to 200 nm) or particle (gray/blue, typical dimensions $<$ 20 nm) morphologies overlaid. Discs' surfaces are largely O-rich (0001) with LiO_2-like surface species, while particles consist of less O-rich (more stoichiometric) Li_2O_2 surfaces. During the initial stage of charging (to $\sim$ 800 mA·h/g_C for discs and to $\sim$ 600 mA·h/g_C for particles), both discs and particles exhibit a sloping voltage profile attributed to solid solution-like surface de-lithiation. Upon further charging, discs and particles exhibit a voltage plateau at $\sim$ 3.4 V vs. Li, corresponding to bulk oxidation via a two-phase process, e.g., between Li_2O_2 and LiO_2.[30]

3.2. OER kinetics

Another key challenge of the aprotic Li-O_2 batteries is their high recharging over-potential (usually $>$ 1 V),[39–43] corresponding to slow kinetics and easily leading to serious side reactions. So it is imperative to understand the kinetics of Li_2O_2 oxidation in aprotic Li^+ electrolytes. The kinetics of OER is affected by the current density and morphology of the discharge products. Adams *et al.*[16] demonstrated that the current density of discharge indirectly influences the charging over-potential by determining the nature and morphology of the Li_2O_2. The charging profiles (Fig. 12(a)) exhibit four regions characterized by distinct differences in slope. Figure 12(b) shows the results of the Li-O_2 cells that were discharged at the same density of 25 mA/cm^2 and then recharged at various rates. All charging profiles are lowered in

over-potential with decreasing charging current density. Figure 12(c) shows that a gradual increase of discharge current also leads to a lower potential region I during charging. The faster discharge yields a charge profile with an extended region I at low potential comparing to the slower discharge (Figure 12(d)).

Recently, Lu *et al.*[31] investigated the reaction kinetics of the charging reactions of aprotic Li-O_2 batteries and found that the OER kinetics is much slower than ORR in Li-O_2 batteries. During Li-O_2 battery charging, OER occurs at high over-potentials (0.4–1.2 V), where the kinetics is sensitive to discharge/charge rates and catalysts, which can be ascribed to the oxidation of bulk Li_2O_2 particles (Fig. 10). Mitchell *et al.*[44] also investigated the rate dependence of the OER over-potential of small particles, plotting the potential after the first 200 mA·h/g_C of charge versus the carbon true surface area normalized current, in a Tafel plot (Fig. 13). The Tafel slope related to charging of small particles was $\sim$ 340 mV per decade. The exchange current density of the OER kinetics of small Li_2O_2 particles was 0.2 nA/cm^2_C, which is an order of magnitude smaller than 1.5 nA/cm^2_C noted on discharge. Viswanathan *et al.*[32] compared the unusual experimental Tafel plots with those obtained by first-principles theory and proposed that minimizing the cell impedance is a more important issue than the intrinsic OER kinetics for developing high rate aprotic Li-O_2 cells (Fig. 5(b)).

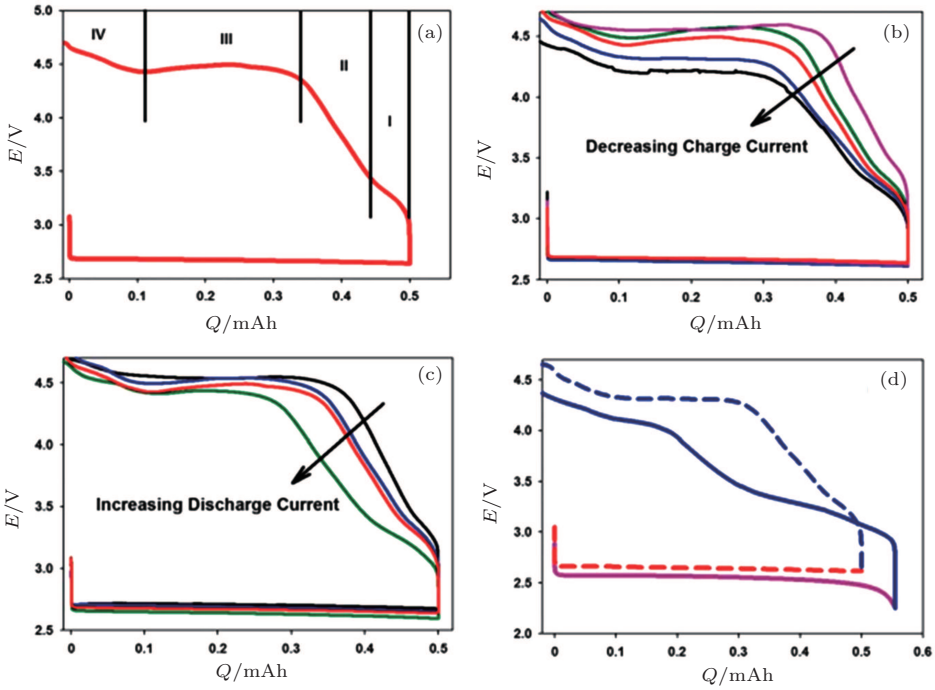


Fig. 12. (a) A discharge–charge curve showing the regions of the charge portion; (b) cells discharged at 25 mA/cm^2 and then charged at different rates from 5–100 mA/cm^2 (colors of curves listed below); (c) cells discharged at different rates from 5–50 mA/cm^2 (colors of curves listed below) and then charged at 25 mA/cm^2; and (d) comparison of a cell fully discharged at 100 mA/cm^2 (pink curve) and then charged at 10 mA/cm^2 with a cell discharged at 25 mA/cm^2 to a similar capacity (red dotted curve) and then charged at 10 mA/cm^2. In panels (b) and (c), black = 5 mA/cm^2, blue = 10 mA/cm^2, red = 25 mA/cm^2, green = 50 mA/cm^2, and pink = 100 mA/cm^2.[16]

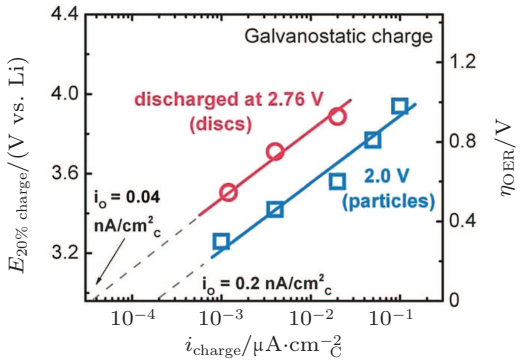


Fig. 13. Tafel plot of galvanostatic charge voltage vs. carbon true surface area-normalized current for electrodes discharged under potentiostatic conditions at 2.76 V or 2.0 V vs. Li to 1000 mA·h/g_C. The right-hand axis shows the OER over-potential referenced to the thermodynamic potential of Li_2O_2, $E^o(Li_2O_2) = 2.96$ V vs. Li.[44]

3.3. Morphology evolution during Li_2O_2 decomposition

A few *in situ* and *ex situ* research facilities having the ability to visualize the Li-O_2 reaction with nanometer resolution were employed to have a closer look at the charging process.[31,43–47] For instance, Zhong *et al.*[35] initially studied the electrochemical oxidation process of Li_2O_2 using *in situ* TEM. Figure 14(a) shows the *in situ* cell schematically assembled in a TEM chamber. The MWCNT/Li_2O_2 positive electrode was prepared by a discharge process. A single Si nanowire electrode was brought into contact with individual Li_2O_2 particles (Fig. 14(b) for a zoom-in view). *In situ* TEM imaging revealed that the preferential oxidation occurs at the MWCNT/Li_2O_2 interface but not at the interface between

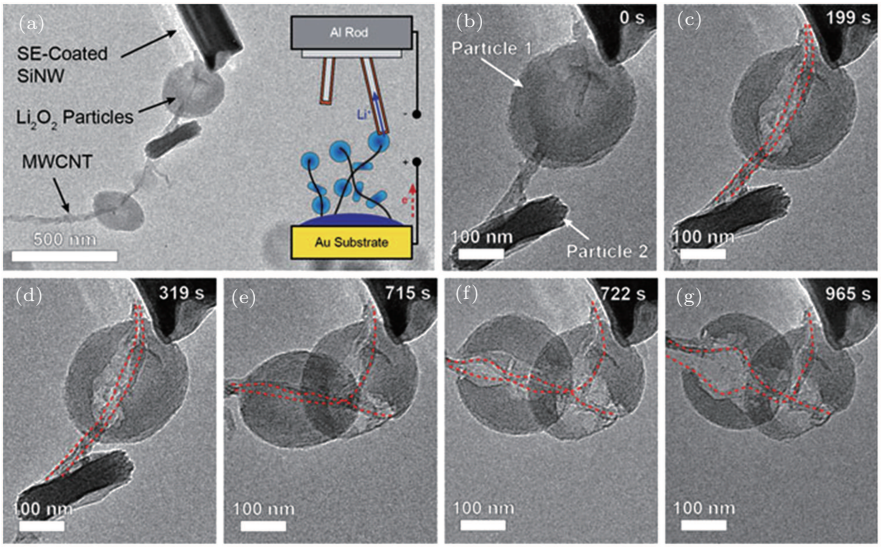


Fig. 14. *In situ* TEM oxidation of Li_2O_2 particles. (a) Schematic illustration of the *in situ* TEM microbattery superimposed over a low magnification TEM image of a solid electrolyte-coated Si nanowire contacting a single Li_2O_2 particle. (b) Higher magnification TEM image of the particles in panel (a), showing a MWCNT bundle contacting two physically separated Li_2O_2 particles labeled as particles 1 and 2, respectively. (c)–(g) Oxidation of particles 1 and 2 during application of a 10 V cell potential to the MWCNT/Li_2O_2 positive electrode against the Si NW negative electrode.[35]

Li_2O_2 and the solid electrolyte (Figs. 14(c)–14(g)). This observation suggests that electron transport in Li_2O_2 ultimately limits the oxidation kinetics at very high over-potentials; however, the experiments with lower over-potentials and longer charging time need to be conducted.

By constructing an all-solid-state Li-O_2 battery in an environmental scanning electron microscope, direct visualization of the discharge and charge processes of the battery was achieved by Zheng *et al.*[48] Different morphologies of the discharge product were observed, including spheres, conformal films, and red-blood-cell-like shapes with the particle size up to 1.5 μm; whereas upon charging, the decomposition initiated at the particle surface and continued along a certain direction, instead of from the contact point at electrode (Fig. 15). These findings indicate that the electron and lithium ion conductivities of Li_2O_2 could support the growth and decomposition of the discharge product in their system.

In situ AFM has also provided clear-cut evidence for decomposition of Li_2O_2 during the charging reaction. Real-time and *in situ* views of the Li_2O_2 decomposition using electrochemical AFM (EC-AFM) are presented in Fig. 16.[49] Details of the decomposition process have been observed at nano-/micrometer scale on a highly oriented pyrolytic graphite (HOPG) electrode. Upon charging, the Li_2O_2 film is decomposed at the interface of Li_2O_2/HOPG and the decomposition potential is related to the thickness of Li_2O_2.

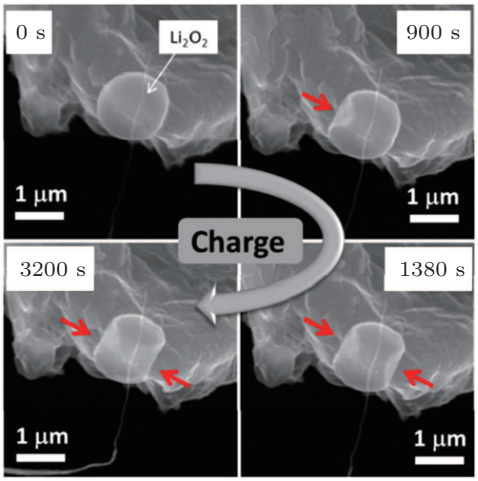


Fig. 15. Charge processes of the Li-O_2 battery. Images captured at 0 s, 900 s, 1800 s, and 3200 s show the decomposition process of the spherical particle. Eight volts was applied on SACNT vs. Li metal to initiate the charge process. Red arrows indicate the position where the particle decomposed. Note that the electron beam was on only during image acquisition, to minimize the irradiation effect.[48]

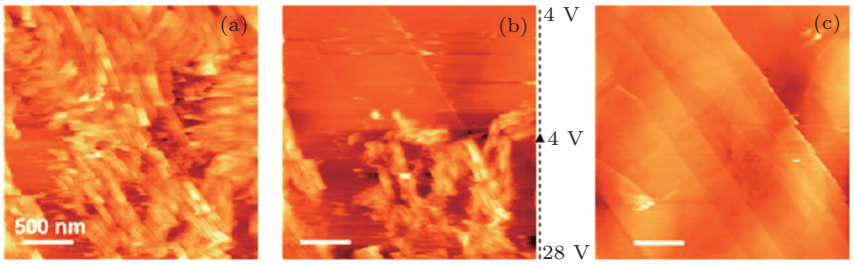


Fig. 16. *In situ* and sequential AFM topographic images of Li_2O_2 nanoplates on HOPG upon OER in Li-O_2 cell. (a) Li_2O_2 nanoplates acquired via the galvanostatic discharge at a cutoff potential of 2.2 V. (b) Potential-dependent view of HOPG electrode from 2.8 V (bottom) to 4.0 V (middle to top) at a sweeping rate of 5 mV/s. (c) Clean HOPG electrode at 4.0 V. The scale bars are 500 nm.[49]

4. Electron and ion transport in Li_2O_2

Among relatively stable aprotic electrolytes, Li_2O_2 has been widely identified as the main discharge product formed in the porous cathode of aprotic Li-O_2 batteries. As Li_2O_2 is an insulator, poor conductivity eventually leads to the so called sudden death at the end of the discharge process. These observations have prompted researchers to investigate the electron and ion transport in Li_2O_2, which are very important for understanding the discharge and charge chemistries involved in Li_2O_2 formation and decomposition mechanisms.[50–54] However, the mechanisms of charge transport through Li_2O_2 remain elusive. Luntz *et al.*[54] presented both experimental and theoretical evidences that hole tunneling generally dominates charge transport through Li_2O_2 in Li-O_2 discharge at practical battery current densities. Others[51,55–58] suggested that diffusion of isolated small polarons trapped at Li vacancies or charged defects governs the charge transport within Li_2O_2. Taken together, these observations motivate the understanding of the mechanism of charge transport through Li_2O_2 mainly determined by two factors:[50,54] (i) the alignment of the Li_2O_2 bands relative to the Fermi level in Li_2O_2 in the electrochemical cell, and (ii) the formation energies, densities, and mobilities of various charged carriers (polarons, vacancies, impurities) at the battery potential.

Figure 17 shows graphically the possible electron and ion transport mechanisms related to the discharge process occurring at the cathode of a Li-O_2 battery. If the ORR process occurs at the Li_2O_2 surface, the charge needs to transport though the discharge product (Figs. 17(a)–17(c)). However, Li_2O_2, the main discharge product, is an insulator with a wide band gap of 4.2–4.5 eV.[55,56] Electronic conductivity is therefore considered to be a major limiter of the capacity of Li-O_2 batteries, because neither tunneling nor bulk conduction can provide appreciable current when the Li_2O_2 film is more than ~ 5 nm thick.[33] Likewise, defects such as surfaces,[57] interfaces,[58] grain boundaries, dislocations, and/or amorphous regions[16] can further enhance conductivity (Fig. 17(c)) for the deposition of large discharge product particles.

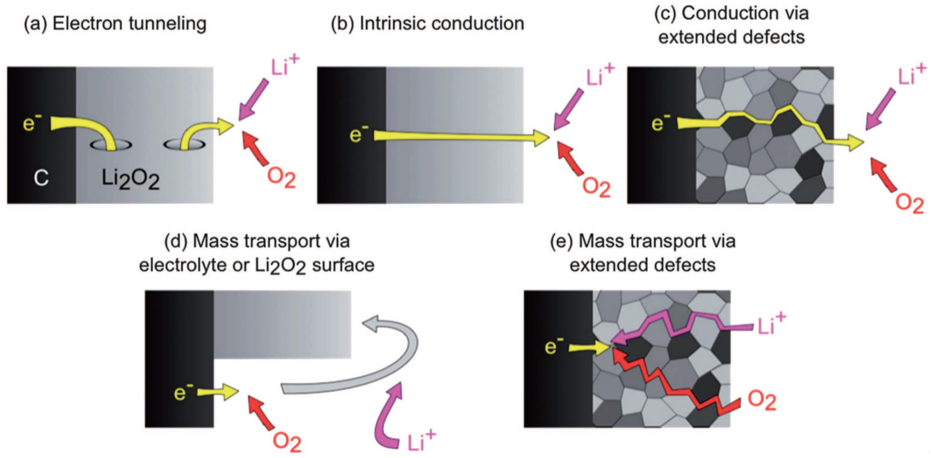


Fig. 17. Possible discharge mechanisms for a Li-O_2 cell.[51]

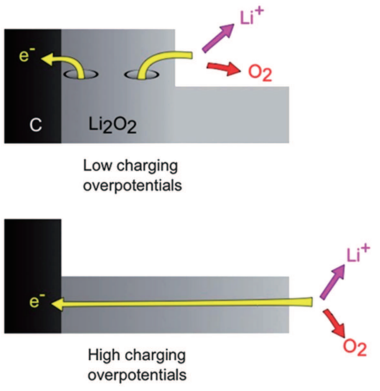


Fig. 18. Proposed two-stage recharge mechanism for a Li-O_2 cell.[51]

Figure 17(d) illustrates a scenario in which ORR happens at the exposed surface of the electrode, followed by diffusion through the electrolyte or along surfaces of existing Li_2O_2. Obviously, the deposition of the Li_2O_2 is not an electrochemical step but rather a chemical one.[56,59] Figure 17(e) illustrates a more exotic mechanism, in which the reduction happens at the buried electrode/Li_2O_2 interface; in this case, the reactants presumably need to diffuse through the products' grain boundaries or other extended defects.

Turning to OER, Figure 18 shows the two-stage electron and ion transport mechanism in the charging process of a Li-O_2 battery. That is, charging may initiate preferentially at a low potential (< 3.5 V) because of dissolution of thin product deposits or decomposition at/near the three-phase electrode/electrolyte/Li_2O_2 boundary. Then, OER will conclude at a high potential in which thick Li_2O_2 decomposes via polaron hopping. More efforts are needed to examine the various possibilities, especially for the location at which ORR and

OER initiate.

5. Conclusion and prospects

This review summarizes the current state of knowledge and research about the fundamental aspects of the oxygen electrode reaction in aprotic Li-O_2 batteries. For the ORRs, O_2 is first reduced via a one-electron process to O_2^-, which transforms to LiO_2 after binding with Li^+ ions and is further reduced to Li_2O_2 through successive electrochemical reduction or chemical disproportionation. However, the oxidation of Li_2O_2 is more complicated, and two different processes have been proposed: the de-lithiation reaction at low over-potentials, and bulk oxidation at higher over-potentials. The kinetics over-potentials for both discharge and recharge are small, regardless of the large potential losses caused by cell impedance. In addition, both hole tunneling and hole polarons contribute to charge transport through Li_2O_2 in aprotic Li-O_2 batteries. Despite some technical challenges currently remaining, fundamental understanding of the mechanisms of oxygen electrode reactions is critical for the further development of aprotic Li-O_2 batteries.

References

[1] Armand M and Tarascon J M 2008 *Nature* **451** 652
[2] Girishkumar G, McCloskey B, Luntz A C, Swanson S and Wilcke W 2010 *J. Phys. Chem. Lett.* **1** 2193
[3] Bruce P G, Freunberger S A, Hardwick L J and Tarascon J M 2012 *Nat. Mater.* **11** 19
[4] Peng Z, Freunberger S A, Chen Y and Bruce P G 2012 *Science* **337** 563
[5] Lu J, Li L, Park J B, Sun Y K, Wu F and Amine K 2014 *Chem. Rev.* **114** 5611
[6] Luntz A C and McCloskey B D 2014 *Chem. Rev.* **114** 11721
[7] Chen Y C, Xie K, Pan Y, Zheng C M and Wang H L 2011 *Chin. Phys. B* **20** 028201
[8] Sun Y, Liu L, Dong J P, Zhao B and Huang X J 2011 *Chin. Phys. B* **20** 126101
[9] Luo G S, Huang S T, Zhao N, Cui Z H and Guo X X 2015 *Chin. Phys. B* **24** 088102
[10] Abraham K M and Jiang Z 1996 *J. Electrochem. Soc.* **143** 1
[11] Débart A, Paterson A J, Bao J and Bruce P G 2008 *Angew. Chem.* **120** 4597
[12] Ma S, Sun L, Cong L, Cong L, Gao X, Yao C, Guo X, Tai L, Mei P, Zeng Y, Xie H and Wang R 2013 *J. Phys. Chem. C* **117** 25890
[13] Freunberger S A, Chen Y, Drewett N E, Hardwick L J, Bardé F and Bruce P G 2011 *Angew. Chem. Int. Ed.* **50** 8609
[14] Chen Y, Freunberger S A, Peng Z, Bardé F and Bruce P G 2012 *J. Am. Chem. Soc.* **134** 7952
[15] OttakamThotiyl M M, Freunberger S A, Peng Z and Bruce P G 2013 *J. Am. Chem. Soc.* **135** 494
[16] Adams B D, Radtke C, Black R, Trudeau M L, Zaqhib K and Nazar L F 2013 *Energy Environ. Sci.* **6** 1772
[17] Fan W, Cui Z and Guo X 2013 *J. Phys. Chem. C* **117** 2623
[18] Hassoun J, Croce F, Armand M and Scrosati B 2011 *Angew. Chem. Int. Ed.* **50** 2999
[19] Kumar J and Kumar B 2009 *J. Power Sources* **194** 1113
[20] Laoire C O, Mukerjee S and Abraham K M 2009 *J. Phys. Chem. C* **113** 20127
[21] Laoire C O, Mukerjee S and Abraham K M 2010 *J. Phys. Chem. C* **114** 9178
[22] Allen C J, Hwang J, Kautz R, Mukerjee S, Plichta E J, Hendrickson M A and Abraham K 2012 *J. Phys. Chem. C* **116** 20755
[23] Trahan M J, Mukerjee S, Plichta E J, Hendrickson M A and Abraham K M 2013 *J. Electrochem. Soc.* **160** A259
[24] Peng Z, Freunberger S A, Hardwick L J, Chen Y, Giordani, V, Bardé F, Novák P, Graham D, Tarascon J M and Bruce P G 2011 *Angew. Chem. Int. Ed.* **123** 6475
[25] Johnson L, Li C, Liu Z, Chen Y, Freunberger S A, Ashok P C, Praveen B B, Dholakia K, Tarascon J M and Bruce P G 2014 *Nat. Chem.* **6** 1091
[26] Frith J T, Russell A E, Garcia-Araez N and Owen J R 2014 *Electrochem. Commun.* **46** 33
[27] McCloskey B D, Scheffler R, Speidel A, Girishkumar G and Luntz A C 2012 *J. Phys. Chem. C* **116** 23897
[28] Abraham K M 2015 *J. Electrochem. Soc.* **162** A3021
[29] Aetukuri N B, McCloskey B D, Garcia J M, Krupp L E, Viswanathan V and Luntz A C 2015 *Nat. Chem.* **7** 50
[30] Gallant B M, Kwabi D G, Mitchell R R, Zhou J, Thompson C V and Shao-Horn Y 2013 *Energy Environ. Sci.* **6** 2518
[31] Lu Y C and Shao-Horn Y 2012 *J. Phys. Chem. Lett.* **4** 93
[32] Viswanathan V, Nørskov J K, Speidel A, Scheffler R, Gowda S and Luntz A C 2013 *J. Phys. Chem. Lett.* **4** 556
[33] Viswanathan V, Thygesen K S, Hummelshøj J S, Nørskov J K, Girishkumar G, McCloskey B D and Luntz A C 2011 *J. Chem. Phys.* **135** 214704
[34] Mitchell R R, Gallant B M, Shao-Horn Y and Thompson C V 2013 *J. Phys. Chem. Lett.* **4** 1060
[35] Zhong L, Mitchell R R, Liu Y, Gallant B M, Thompson C V, Huang J Y, Mao C X and Shao-Horn Y 2013 *Nano Lett.* **13** 2209
[36] Ogasawara T, Débart A, Holzapfel M, Novak P and Bruce P G 2006 *J. Am. Chem. Soc.* **128** 1390
[37] Yang J, Zha D, Wang H H, Lau, K C, Schlueter J A, Du P, Myers D J, Sun, Y K, Curtiss, L A and Amine K 2013 *Phys. Chem. Chem. Phys.* **15** 3764
[38] Yang X and Xia Y 2010 *J. Solid State Electrochem.* **14** 109
[39] Hummelshøj J S, Blomqvist J, Datta S, Vegge T, Rossmeisl J, Thygesen K S, Luntz A C, Jacobsen KWand Norskov J K 2010 *J. Chem. Phys.* **132** 071101
[40] McCloskey B D, Scheffler R, Speidel A, Bethune D S, Shelby R M and Luntz A C 2011 *J. Am. Chem. Soc.* **133** 18038
[41] Sun B, Wang B, Su D, Xiao L, Ahn H and Wang G 2012 *Carbon* **50** 727
[42] Højberg J, McCloskey B D, Hjelm J, Vegge T, Johansen K, Norby P and Luntz A C 2015 *ACS Appl. Mater. Inter.* **7** 4039
[43] Herrera S E, Tesio A Y, Clarenc R and Calvo E J 2014 *Phys. Chem. Chem. Phys.* **16** 9925
[44] Mitchell R R, Gallant B M, Thompson C V and Shao-Horn Y 2011 *Energy Environ. Sci.* **4** 2952
[45] Feng N, He P and Zhou H 2015 *ChemSusChem* **8** 600
[46] Yadegari H, Li Y, Banis M N, Li X, Wang B, Sun Q and Sun X 2014 *Energy Environ. Sci.* **7** 3747
[47] Harding, J R, Lu Y C, Tsukada Y and Shao Horn Y 2012 *Phys. Chem. Chem. Phys.* **14** 0540
[48] Zheng H, Xiao D, Li X, Liu Y, Wu Y, Wang J, Jiang K, Chen C, Gu L, Wei X, Hu Y, Chen Q and Li H 2014 *Nano Lett.* **14** 4245
[49] Wen R, Hong M and Byon H R 2013 *J. Am. Chem. Soc.* **135** 10870
[50] Varley, J B, Viswanathan V, Nørskov J K and Luntz A C 2014 *Energy Environ. Sci.* **7** 720
[51] Radin M D and Siegel D J 2013 *Energy Environ. Sci.* **6** 2370
[52] Geng W T, He B L and Ohno T 2013 *J. Phys. Chem. C* **117** 25222
[53] Tian F, Radin M D and Siegel D J. 2014 *Chem. Mater.* **26** 2952
[54] Luntz A C, Viswanathan V, Voss J, Varley J B, Nørskov J K, Scheffler R and Speidel A 2013 *J. Phys. Chem. Lett.* **4** 3494
[55] Ong S P, Mo Y and Ceder G 2012 *Phys. Rev. B* **85** 081105
[56] Kang J, Jung Y S, Wie S and Dillon A C 2012 *Phys. Rev. B* **85** 035210
[57] Radin M D, Rodriguez J F, Tian F and Siegel D J 2012 *J. Am. Chem. Soc.* **134** 1093
[58] Zhao Y, Ban C, Kang J, Santhanagopalan S, Kim G H, Wei S H and Dillon A C 2012 *Appl. Phys. Lett.* **101** 023903
[59] Lu Y C, Gallant B M, Kwabi D G, Harding J R, Mitchell R R, Whittingham M S and Shao Horn Y 2013 *Energy Environ. Sci.* **6** 750